IEEE Access
Multidisciplinary | Rapid Review | Open Access Journal

Received 22 June 2023, accepted 26 June 2023, date of publication 30 June 2023, date of current version 12 July 2023.

Digital Object Identifier 10.1109/ACCESS.2023.3291345

RESEARCH ARTICLE

The Effect of Sand and Dust Storms (SDSs) and Rain on the Performance of Cellular Networks in the Millimeter Wave Band

MARYAM OLYAEE[1], MOHSEN ESLAMI[2], KEIVAN NAVAIE[3], (Senior Member, IEEE), JUAN M. ROMERO-JEREZ[1], (Senior Member, IEEE), HADI HASHEMI[4], JAVAD HAGHIGHAT[5], AND MOHAMAD BAHMANPOUR[2]

[1]Telecommunication Research Institute (TELMA), E.T.S. Ingeniería de Telecomunicación, University of Malaga, 29010 Málaga, Spain
[2]Department of Electrical Engineering, Shiraz University of Technology, Shiraz 71557-13876, Iran
[3]School of Computing and Communications, Lancaster University, LA1 4WA Lancaster, U.K.
[4]Department of Signal Theory, Telematics and Communications, University of Granada, 18071 Granada, Spain
[5]Department of Electrical and Electronics Engineering, TED University, 06420 Ankara, Turkey

Corresponding author: Keivan Navaie (k.navaie@lancaster.ac.uk)

This work was supported in part by the Engineering and Physical Sciences Research Council (EPSRC) under Grant EP/K/022725/1. The work of Maryam Olyaee and Juan M. Romero-Jerez was supported in part by the Junta de Andalucia under Project P21-00420.

ABSTRACT Future cellular systems are expected to use millimeter-wave (mm-Wave) frequency bands in addition to the existing microwave bands under 6 GHz. Severe weather conditions, including sand and dust storms (SDSs) and heavy rainfalls, challenge reliable communications over wireless links at those higher frequencies. In such conditions, besides frequency-dependent path-loss, radio signals experience additional attenuation. The SDS attenuation is related to visibility, receiver distance to the storm origin point, soil type, frequency, temperature and humidity. On the other hand, the rainfall attenuation is affected by rainfall rate, polarization, carrier frequency, temperature and raindrop size distribution. Leveraging on experimental measurements carried out in previous works, a novel unified mathematical framework is introduced in this paper to include SDS/rainfall-dependent attenuation in the performance evaluation of terrestrial wireless cellular networks in terms of coverage probability, bit error rate (BER) and achievable rate in the mm-Wave band. Extensive numerical results are presented to show the effects of the different SDS/rainfall parameters on performance, showing that the degradation due to SDS is generally higher than that due to rain and may cause a reduction of even six orders of magnitude in the average achievable bit rate when the frequency increases from 28 to 38 GHz.

INDEX TERMS Cell planning, cellular networks, mm-wave band, performance analysis, rainfall, sand and dust storm.

I. INTRODUCTION

Due to the high demands and expectations envisioned for future generations of cellular networks, exploiting higher frequencies in the mm-Wave bands seems to be inevitable [1]. Furthermore, the forthcoming 5th generation (5G) cellular communications technology is a diverse and heterogeneous network in terms of base stations (BSs) and operating frequency bands. Machine-to-machine (M2M) [2], device-to-device (D2D) [3], and low power wide area (LPWA) communications are examples of what 5G is supporting. In general, most research in the aforementioned areas in the context of 5G heterogeneous networks assume regular weather conditions. Since 5G is going to be deployed worldwide, it is critical to investigate cellular networks' performance in extreme weather conditions, such as heavy rainfalls and sand and dust storms (SDSs).

The main effect of rainfall and precipitation on wireless signal transmission is an increase of signal attenuation [4], [5], which is usually quantified in terms of the measured

The associate editor coordinating the review of this manuscript and approving it for publication was Stefan Schwarz.

rain rate during a given time percentage. Attenuation per unit length curves for frequencies between 3 and 100 GHz for different rainfall rates can be found in [6]. Also, scattering and *phase fluctuations* effects caused by rainfall on the performance of a wireless link using multiple antennas has been investigated [7]. The attenuation and scattering in radio links due to rain is predicted from rainfall rate statistics with a 1-min integration, and a method to obtain the rainfall rate exceeded for any given time percentage and for any location at 1-min integration time has been established by ITU-R and presented in [8]. Also, methods to estimate 1-min rain rate by making a better use of the available data are discussed in [9] and [10]. In [11] a modified effective rainfall rate method is proposed to include the prevailing wind direction during rainy conditions as an additional parameter for the prediction of rain attenuation. Studies on attenuation due to rainfall have shown that, in non-tropical regions with rainfall rates lower than 100 millimeter per hour (mm/h), the attenuation due to rainfall does not contribute significantly to the overall path loss for short distance wireless links below 200 m [5]. However, for higher frequencies or distances, or in tropical areas with rainfall rates above 100 mm/h, the attenuation due to rain cannot be ignored. For instance, for a Tx-Rx (transmitter to receiver) distance of 200 m with a rainfall rate of 25 mm/h at 28 GHz, the rain attenuation is 1.4 dB, which can be neglected when compared to the distance-dependent path loss of around 80 dB. However, the rainfall rate in tropical areas such as Kolkata, India, reaches 100 mm/hour at almost 0.01% of the time, which causes a significant attenuation, greater than 10 dB, for the mentioned 200 m distance at 28 GHz [5]. In [12], rain attenuation and drop size distribution measurements are presented at 77 and 300 GHz for up to 20 mm/h rainfall rate. Intense heavy rainfall and large raindrop sizes are studied in [13], [14], and [15]. In [13], the rain rate and rain attenuation at 26 GHz are evaluated by means of experimental measurements in Malaysia on a 5G microwave radio link, and rainfall is categorized based on drizzle, showers and thunderstorms according to its rainfall rate and compared with ITU-R predictions, reporting a total rain attenuation over 1.3 km of 34 dB, while results in [14] show that 18.4 dB/km of rain attenuation can be expected at 38 GHz. Also in Malaysia, the rainfall attenuation is investigated in [16] at 38 GHz, where measurement data were simultaneously collected for rainfall rate and received signal level in 1-minute time over a 300 m path length, reporting an attenuation of 15 dB for an average rain rate of 125 mm/h, which was obtained at 0.01% of the time, while the rain attenuation can be as high as 25.78 dB for a rain rate of 210 mm/h [17]. On the other hand, the rain attenuation fitting distribution at 25.84 and 77.52 GHz mm-Wave 5G bands are studied in [18], and the collected measurement data are presented for short-range links over a year. Additionally, a one-year rain attenuation measurement at 73.5 GHz for a 1.8 km link is presented in [19] that resulted in a maximum attenuation of 40.1 dB for a maximum rain rate of 108 mm/h.

While some parts of the world face heavy rainfalls and precipitations, in other areas SDSs constitute a major challenge for reliable wireless transmission. Wide semi-desert regions and areas with sparse vegetation in America, North Africa and the Middle East experience this harsh atmospheric conditions. Moreover, desertification due to natural or anthropogenic factors results in an increasing rate of occurrence of SDSs [20], [21], [22]. In these areas, small sand or dust particles[1] can be lifted a few meters above the ground level during an SDS, which reduces visibility and, in extreme cases, causes interruption of public services such as power lines and telecommunication networks. SDSs are often characterized in terms of the ''Visibility'' parameter, which depends on the distance of the point of interest to the source of the storm and the height of the point of interest from the ground level. It is also related to the mass of dust per cubic meter of air and is given in kilometers unit [23]. Thus, wireless communication channel characteristics change in SDS conditions, and, accordingly, the performance of operating wireless systems is affected, as an extra attenuation due to SDS has to be considered, for which different models can be found in the related technical literature. The SDS attenuation has been usually estimated using the Rayleigh approximation [24], [25], [26] and the Mie solution to Maxwell's equations (Mie scattering) [27], [28], [29] for solving the forward scattering amplitude function of a single particle. These methods assume specific particles geometries (spheres, ellipsoids, cubes, etc.) and do not include multiple scattering effect or mutual interaction among particles and their random distribution and orientation. Also, although it is known that the size distribution of dust particles in an SDS can be characterized with a lognormal distribution [26], most SDS attenuation models relay on deterministic values of the Visibility parameter. For these reasons, alternative approaches to SDS attenuation estimation have been proposed, including empirical [30] and statistical [31] models. In our work, we have used the approach in [32] to model SDS attenuation, which is obtained by using the effective material property technique.

Coverage, achievable throughput and bit error rate (BER) are important performance metrics for cellular networks [33], [34], [35], which are greatly affected by the channel characteristics between the BS and the user equipment (UE). In this regard, rainfall and SDS result in a decrease of the received signal-to-noise ratio (SNR) compared to the clear sky situation. As these atmospheric conditions become more frequent due to global warming, they have to be considered in the design of cellular networks, which were originally designed and deployed without considering such phenomena. For the users, this consequently results in a lower than expected coverage and average achievable throughput, as well as a higher error rate. Performance analysis papers considering rainfall and SDS are very scarce. The effect of SDS on the attenuation

[1] Particles with a radius smaller than 60 μm are defined as dust, and larger than that are referred to as sand [23].

of GSM signals is studied in [35], while the impact of rainfall have been investigated for the performance of wireless power transfer [36] and BER in a point-to-point wireless link [37]. To the best of our knowledge, no prior work has investigated coverage, achievable throughput and BER degradation of cellular networks due to rainfall and SDS. This is however an immediate need as the performance evaluation of these metrics provide insights on the effect of harsh atmospheric conditions on network design and the cost of alleviating such conditions on network performance.

In this paper a novel unified mathematical framework is introduced to include SDS/rainfall-dependent attenuation in the performance evaluation of wireless cellular systems in terms of coverage, achievable throughput and BER. We assume the location of BSs to be modeled by a Poisson point process (PPP), which is considered in the context of stochastic geometry [38] and which is more realistic than a grid type of BS deployment. We then use distance, precipitation and visibility-dependent path-loss models to evaluate the aforementioned performance metrics at mm-Wave bands. Moreover, multipath propagation results in the reception of multiple replicas of the transmitted signal causing fast variations of the received power as users move. This multipath fading is known to generally have a detrimental impact on cellular performance and it is explicitly considered in the presented analysis, which also constitutes a novelty with respect to previous SDS/rainfall related works. Our analysis provides exact expressions for the degradation of performance metrics as a function of the parameters characterizing the network layout and the instantaneous channel gain. The developed approach further enables network designers with options (e.g., the average number of extra BSs to be deployed per unit area and/or higher BS transmit power) to compensate for the performance degradation due to SDS and rainfall. Specifically, the following key contributions are presented in this paper:

- Exact mathematical expressions are derived for the coverage probability, achievable bit rate and BER of terrestrial wireless cellular networks in the mm-Wave band assuming random BS locations, frequency-dependent path-loss, SDS/rainfall attenuation and Rayleigh multipath fading. The attenuation (in dB/km) due to SDS and rainfall is used as input parameter.
- Extensive numerical results are presented to show the effects of the different SDS/rainfall parameters on performance of the analyzed cellular networks at the system level.
- The cost of provisioning a certain level of performance, in terms of the excess transmission power at the BSs, in the presence of SDS or rainfall is analyzed.

The rest of the paper is organized as follows: Section II describes the system and channel models. Section III presents mathematical derivations for evaluating coverage, achievable rate and BER degradation in terms of visibility and rainfall rate. In Section IV, simulation results are presented, followed by the conclusions in Section V.

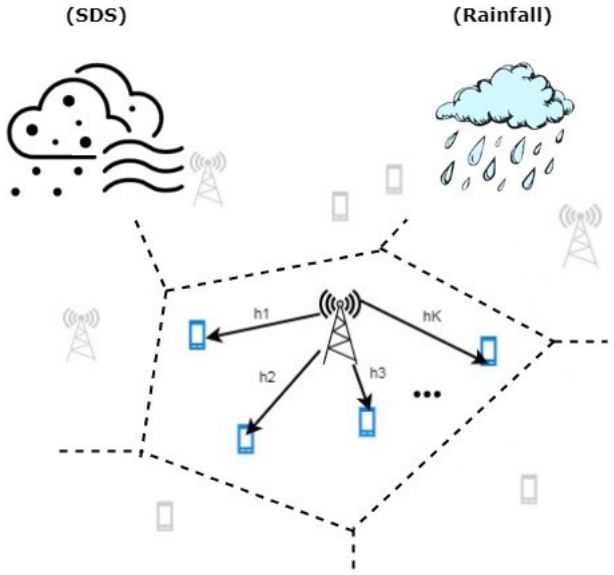

FIGURE 1. A sample cellular network layout in downlink with Voronoi cells for K users, used for performance analysis of SDS/rainfall weather conditions.

II. SYSTEM AND CHANNEL MODEL

We consider the downlink of a cellular network where the BSs are distributed throughout the network according to a homogeneous 2-dimensional Poisson point process (PPP) that results in Voronoi cells [38], Φ, with density λ (number of BSs per unit area). It is assumed that UEs connect to their closest BS, which are considered to be equipped with omni-directional antennas. Users are also assumed to be distributed according to a PPP distribution, Φ_u, with density λ_u (number of users per unit area). Distributions Φ and Φ_u are assumed to be mutually independent. The probability density function (PDF) of the distance between a user and its nearest BS, r, is then expressed as follows [39]:

$$f_R(r) = 2\pi\lambda r \exp(-\lambda\pi r^2). \tag{1}$$

It is further assumed that the BS transmit power is P watts and UEs are allocated orthogonal channels via one of the orthogonal multiple access schemes, hence there is no inter-user interference.

A. SAND/DUST AND RAINFALL DEPENDENT PATH-LOSS MODELS

1) SAND AND DUST

The severity of SDSs is often characterized in terms of the visibility parameter, V, which is expressed, in kilometers, as [23]

$$V = \sqrt[\rho_s]{C_s/M}, \tag{2}$$

where M is the mass of sand and dust in kilograms per cubic meter of air, and C_s and ρ_s are constants that depend on the distance of the receiver to the storm's origin point, type of soil and climate conditions.

We follow in this subsection the approach in [32] to characterize the signal attenuation due to SDS. Assuming the

mass density of soil particles to be m_d, the volume fraction occupied by sand and dust particles in a storm is obtained as

$$V_f = m_d / V^{\rho_s}. \tag{3}$$

The *equivalent* complex relative permittivity of SDSs is calculated as

$$\begin{aligned}\epsilon^*_{\rm eq} &= \epsilon_{\rm air} + \frac{3V_f \times \epsilon_{\rm air}(\epsilon^*_{\rm sd} - \epsilon_{\rm air})/(\epsilon^*_{\rm sd} + 2\epsilon_{\rm air})}{1 - V_f(\epsilon^*_{\rm sd} - \epsilon_{\rm air})/(\epsilon^*_{\rm sd} + 2\epsilon_{\rm air})} \\ &\triangleq \hat{\epsilon}_{\rm eq} - j\bar{\epsilon}_{\rm eq}.\end{aligned} \tag{4}$$

where $\epsilon^*_{\rm sd}$ is the complex relative permittivity of sand and dust, for which a number of frequency-dependent values in the range of $3 - 100$ GHz are given in [32], and $\epsilon_{\rm air}$ is the relative dielectric constant of air. Using (4), the SDS-dependent path-loss in dB is also given in [32] as

$$\begin{aligned}\zeta_{k,\rm dB}(V, r) &= \frac{k_v}{\lambda_0}\left[\frac{\hat{\epsilon}_{\rm eq}}{2}\left(\sqrt{1+\tan^2\delta} - 1\right)\right]^{0.5} r, \\ &\triangleq \Theta_{\rm SDS} \times r,\end{aligned} \tag{5}$$

where $\Theta_{\rm SDS}$ is given in dB/km, $k_v = 0.017372\pi$, $\tan\delta = \bar{\epsilon}_{\rm eq}/\hat{\epsilon}_{\rm eq}$, and λ_0 is the wavelength of the radio wave.

2) RAINFALL

The attenuation due to rain, $\Theta_{\rm Rain}$, in (dB/km), is obtained using a power-law relationship as [4] and [40]

$$\Theta_{\rm Rain} = a_{Rain} \times \tilde{R}^{b_{Rain}}, \tag{6}$$

where $\tilde{R}$ is the rain rate in mm/h and a_{Rain} and b_{Rain} are parameters. Thus, the rainfall-dependent path-loss is expressed as

$$\zeta_{k,\rm dB}(\tilde{R}, r) = \Theta_{\rm Rain} \times r, \tag{7}$$

where r is given in km, and parameters a_{Rain} and b_{Rain} are a function of different factors such as polarization, carrier frequency, temperature and raindrop size distribution, which can be obtained from experimental measurements [4].

Values for a_{Rain} and b_{Rain} for horizontal, vertical and circular polarization, and for all path geometries, are calculated in [40], for frequencies, f (GHz), in the range 1-1000 GHz, as

$$\begin{aligned}\log_{10}(a_{Rain}) = &\sum_{j=1}^{4}\left(a_j \exp\left[-\left(\frac{\log_{10} f - b_j}{c_j}\right)^2\right]\right) \\ &+ m_a \log_{10} f + c_a,\end{aligned} \tag{8}$$

$$\begin{aligned}b_{Rain} = &\sum_{j=1}^{5}\left(a_j \exp\left[-\left(\frac{\log_{10} f - b_j}{c_j}\right)^2\right]\right) \\ &+ m_b \log_{10} f + c_b,\end{aligned} \tag{9}$$

where values for the coefficient constant a_j, b_j, c_j, m_a, c_a, m_b and c_b are given in Tables 1-4 in [40].

The rain rate provides a measure to characterize different rainfall environments. Thus, for heavy rains, $10 \le \tilde{R} \le 50$ mm/h is expected, whereas in tropical areas $\tilde{R}$ reaches higher values [41]. For instance, in Malaysia, due to its tropical location, the monthly average rain rate is around 200 mm/h during the wet season [42].

B. CHANNEL MODEL

The complex baseband signal amplitude of the frequency-flat fading channel between the k-th UE to its corresponding BS can be expressed as [43]

$$h_k = \sqrt{\frac{1}{\alpha_k(r)\zeta_k(r)}} h_{w,k}, \quad 1 \le k \le K, \tag{10}$$

where $\alpha_k(r)$ and $\zeta_k(r)$ denote, respectively, the distance-dependent and rainfall/SDS-related attenuation, K denotes the total number of users in a cell, r denotes the UE-BS distance and $h_{w,k}$ denotes the channel's small scale Rayleigh fading, i.e., $h_{w,k}$s are independent and identically distributed (i.i.d.) zero-mean, unit-variance complex Gaussian random variables, $\mathcal{CN}(0, 1)$.

In the case of SDS, $\zeta_k(r)$ is a function of the visibility (V) in the area where user k is located. In the case of rainfall, $\zeta_k(r)$ is a function of the rainfall rate ($\tilde{R}$). Fig. 1 shows a sample cellular network downlink layout in these conditions.

For the distance dependent path-loss in millimeter-wave frequencies, we adopt the model given in [44] as follows:

$$\alpha_{k(\rm dB)}(r) = A + B \times 10\log_{10}(r), \tag{11}$$

where parameters A and B depend on BS and UE heights, and non-line-of-sight (NLOS) channels are assumed. Table 1 shows path loss parameters, A and B, for measurements collected in New York City at 28 GHz and Austin, Texas, at 38 GHz, with different BS antenna heights [44].

TABLE 1. Parameters of Path Loss for different frequencies for NLOS channels [44].

Frequency	TX Height (meter)	RX Height (meter)	B	A (dB)
28 GHz	7	1.5	3.73	75.85
28 GHz	17	1.5	4.51	59.89
38 GHz	8	1.5	1.28	115.17
38 GHz	23	1.5	0.12	118.77
38 GHz	36	1.5	0.41	116.77

In order to evaluate network's performance, we now define an overall attenuation parameter which depend on distance r, encompassing distance-dependent path-loss ($\alpha_{k,dB}$) and SDS/rainfall attenuation ($\zeta_{k,dB}$).

Definition: The overall attenuation due to distance and rainfall/SDS-based path-loss for the k-th user is expressed as

$$\begin{aligned}L_{k,\rm dB}(r) &\triangleq \alpha_{k,\rm dB}(r) + \zeta_{k,\rm dB}(r) \\ &= \mathcal{L}_{\rm c} + \mathcal{L}_{\rm lg}\ln(r) + \mathcal{L}_{\rm l} r,\end{aligned} \tag{12}$$

where

$$\mathcal{L}_{\rm c} = A, \tag{13a}$$

$$\mathcal{L}_{\rm lg} = \frac{10B}{\ln(10)}, \tag{13b}$$

$$\mathcal{L}_{\rm l} = \begin{cases}\Theta_{\rm SDS}, & \text{for SDS,} \\ \Theta_{\rm Rain}, & \text{for rainfall.}\end{cases} \tag{13c}$$

Equation (12) shows that the total power loss in dB is a function of r and $ln(r)$, whereas in clear sky conditions only the dependence on $ln(r)$ is present, i.e., the distance dependent path-loss in watts is a function of r^B in the latter case.

Simultaneously considering both SDS/rainfall and distance-dependent attenuation in network performance analysis is a novel contribution of this work, yielding accurate and realistic results for the assumed harsh propagation conditions. For all environment related parameters of $L_{k,\mathrm{dB}}(r)$, we use values obtained from experimental measurements in the mm-Wave band given in [32], [40], and [44].

III. PERFORMANCE ANALYSIS

We use a cellular downlink network model and an SDS/rainfall attenuation-dependent channel model for the performance analysis carried out in this section in terms of coverage probability, average achievable rate and BER.

The received SNR at the k-th user considering SDS/rainfall is given by

$$\Gamma_k = \frac{P|h_k|^2}{N_0} = \frac{P|h_{w,k}|^2}{N_0 10^{L_{k,\mathrm{dB}}(r)/10}}, \tag{14}$$

where P is the BS transmitted power, in watts, incorporating all power gains and losses (antenna gains, cable losses, etc.) and N_0 is the noise power at the receiver.

A. COVERAGE PROBABILITY

The coverage probability under SDS/rainfall is defined as [45]

$$P_{\mathcal{C}}(T) \triangleq \mathbb{E}\left\{\Pr\{\Gamma_k > T\}\right\}, \tag{15}$$

where T is a predefined threshold that depends on the receivers' sensitivity, and $\mathbb{E}$ represents the expected value with respect to distance r, distributed according to (1), and fading. The coverage probability without SDS/rainfall is defined as $\hat{P}_{\mathcal{C}}(T) = \mathbb{E}\left\{\Pr\{\hat{\Gamma}_k > T\}\right\}$, where $\hat{\Gamma}_k = \frac{P|h_{w,k}|^2}{N_0 10^{\hat{L}_{k,\mathrm{dB}}(r)/10}}$, and $\hat{L}_{k,\mathrm{dB}}(r) = \mathcal{L}_{\mathrm{c}} + \mathcal{L}_{\mathrm{lg}} \ln(r)$.

Proposition 1: Let $P_{\mathcal{C}}(T)$ and $\hat{P}_{\mathcal{C}}(T)$ be, respectively, the coverage probability under SDS/rainfall and in normal weather conditions, i.e., without SDS/rainfall. The average degradation of coverage probability in a cellular network in SDS or rainfall conditions is given by

$$\begin{aligned}\Delta P_{\mathcal{C}}(T) &= \hat{P}_{\mathcal{C}}(T) - P_{\mathcal{C}}(T) \\ &= \sum_{k=0}^{\infty}\sum_{j=0}^{\infty} -\frac{(-\mu_0)^k (k\mu_2)^j}{k!j!}(\lambda\pi)^{-\frac{k\mu_1+j}{2}}\Gamma \\ &\quad \times \left(\frac{k\mu_1+j+2}{2}\right) \\ &\quad + \frac{(-\mu_0)^k}{k!}(\lambda\pi)^{-\frac{k\mu_1}{2}}\Gamma\left(\frac{k\mu_1+2}{2}\right),\end{aligned} \tag{16}$$

where $\Gamma(\cdot)$ is the Gamma function [46, eq. (6.1.1)] and

$$\mu_0 = \frac{TN_0}{P}10^{\mathcal{L}_c/10}, \tag{17a}$$

$$\mu_1 = \frac{\ln(10)}{10}\mathcal{L}_{\mathrm{lg}}, \tag{17b}$$

$$\mu_2 = \frac{\ln(10)}{10}\mathcal{L}_l, \tag{17c}$$

Proof: See Appendix. □

Note that, according to Proposition 1, the extreme case of deploying a large enough number of BSs, $\lambda \to \infty$, yields $\Delta P_{\mathcal{C}} \to 0$. Furthermore, the factorial of summation indexes in the denominator and the negative exponents of the power functions make the terms of (16) to rapidly decrease to zero; requiring only a few terms of the infinite sum to be evaluated.

B. ACHIEVABLE RATE

The average achievable rate is defined as

$$\overline{R} = \mathbb{E}\{\log_2(1+\Gamma_k)\}, \tag{18}$$

and the degradation of the average achievable rate ($\Delta\overline{R}$) is defined as the difference between the achievable rates in clear sky, $\overline{R}_0$, and with SDS/rainfall, $\overline{R}$, i.e.,

$$\Delta\overline{R} = \mathbb{E}\{\log_2(1+\hat{\Gamma}_k)\} - \mathbb{E}\{\log_2(1+\Gamma_k)\}. \tag{19}$$

Proposition 2: The average achievable rate degradation in cellular network under SDS/rainfall is obtained as

$$\begin{aligned}\Delta\overline{R} = \overline{R}_0 + \int_0^{\infty} &\frac{2\pi\lambda}{\ln(2)}\exp(\tilde{\mu}_0 r^{\tilde{\mu}_1}\exp(\tilde{\mu}_2 r) - \pi\lambda r^2) \\ &\times \mathrm{Ei}\left(-\tilde{\mu}_0 r^{\tilde{\mu}_1}\exp(\tilde{\mu}_2 r)\right) r dr,\end{aligned} \tag{20}$$

with

$$\overline{R}_0 = \int_0^{\infty} \frac{-2\pi\lambda}{\ln(2)}\exp(\tilde{\mu}_0 r^{\tilde{\mu}_1} - \pi\lambda r^2)\mathrm{Ei}\left(-\tilde{\mu}_0 r^{\tilde{\mu}_1}\right) r dr, \tag{21}$$

where $Ei(\cdot)$ is the exponential integral function defined, for real-valued $x \neq 0$, as $Ei(x) \triangleq -\int_{-x}^{\infty}\frac{e^{-t}}{t}dt$ and where

$$\tilde{\mu}_0 = \frac{N_0}{P}10^{\mathcal{L}_c/10}, \tag{22a}$$

$$\tilde{\mu}_1 = \frac{\ln(10)}{10}\mathcal{L}_{lg}, \tag{22b}$$

$$\tilde{\mu}_2 = \frac{\ln(10)}{10}\mathcal{L}_l. \tag{22c}$$

Proof: The achievable rate is obtained by averaging over the Rayleigh fading and the UE-BS distance distributions. Thus, we can write

$$\begin{aligned}\overline{R}(P, N_0, \lambda) &= \mathbb{E}\{\log_2(1+\Gamma_k)\} \\ &= \mathbb{E}_r\left\{\int_0^{\infty}\log_2\left(1+\frac{P\gamma}{N_0 10^{L_{k,\mathrm{dB}}(r)/10}}\right)e^{-\gamma}d\gamma\right\},\end{aligned} \tag{23}$$

which can be rewritten in terms of the defined constants $\tilde{\mu}_0$, $\tilde{\mu}_1$ and $\tilde{\mu}_2$ as

$$\begin{aligned}
&\overline{R}(P, N_0, \lambda) \\
&= \mathbb{E}_r \left\{ \int_0^{\infty} \log_2 \left(1 + \frac{\gamma}{\tilde{\mu}_0 r^{\tilde{\mu}_1} \exp(\tilde{\mu}_2 r)} \right) e^{-\gamma} d\gamma \right\} \\
&= \mathbb{E}_r \left\{ \frac{-\exp(\tilde{\mu}_0 r^{\tilde{\mu}_1} \exp(\tilde{\mu}_2 r))}{\ln(2)} \mathrm{Ei}\left(-\tilde{\mu}_0 r^{\tilde{\mu}_1} \exp(\tilde{\mu}_2 r) \right) \right\} \\
&= \int_0^{\infty} \frac{-2\pi\lambda}{\ln(2)} \exp(\tilde{\mu}_0 r^{\tilde{\mu}_1} \exp(\tilde{\mu}_2 r) - \pi\lambda r^2) \\
&\quad \times \mathrm{Ei}\left(-\tilde{\mu}_0 r^{\tilde{\mu}_1} \exp(\tilde{\mu}_2 r) \right) r dr. \qquad (24)
\end{aligned}$$

Also, $\overline{R}_0$ is obtained by setting $\tilde{\mu}_2 = 0$ in (24). Defining $\Delta\overline{R}$ as in (19) it is then straightforward to obtain (20). □

C. BIT ERROR RATE

For a particular realization of the instantaneous SNR Γ_k at the receiver, the BER for PSK and QAM modulations is given by [47]

$$P_b = \sum_{m=1}^{M} \alpha_m Q(\sqrt{2\beta_m \Gamma_k}), \qquad (25)$$

where $Q(\cdot)$ is the Gaussian Q-function, and parameters M, α_m and β_m depend on the modulation type. As the SNR Γ_k is a random variable, the average BER can be calculated by promediating (25) over the fading distribution [45, Chap. 6] as well as over the distribution of the distance between the considered user and its nearest BS, i.e.,

$$P_{\mathcal{E}} = \int_0^{\infty} \int_0^{\infty} P_{b|\Gamma_k(\gamma,r)} f_{\gamma}(\gamma) f_R(r) d\gamma dr, \qquad (26)$$

where, from (14), $\gamma \triangleq |h_{k,w}|^2$ follows a unit-mean exponential distribution and $f_{\gamma}(\cdot)$ denotes its PDF, and $f_R(\cdot)$ is given in (1).

Proposition 3: The average BER in SDS/rainfall conditions in a cellular network is calculated as

$$P_{\mathcal{E}} = \sum_{m=1}^{M} \alpha_m \left(\frac{1}{2} - \pi\lambda \int_0^{\infty} \sqrt{\frac{\beta_m}{\tilde{\mu}_0 r^{\tilde{\mu}_1} e^{\tilde{\mu}_2 r} + \beta_m}} r e^{-\lambda\pi r^2} dr \right), \qquad (27)$$

Proof: Introducing (1) and (25) into (26), and also considering $f_{\gamma}(\gamma) = e^{-\gamma}$, we can write

$$\begin{aligned}
P_{\mathcal{E}} &= \int_0^{\infty} \int_0^{\infty} \sum_{m=1}^{M} \alpha_m Q\left(\sqrt{\frac{2\beta_m P \gamma}{N_0 10^{L_{k,dB}(r)/10}}} \right) \\
&\quad \times e^{-\gamma} 2\pi\lambda r e^{-\lambda\pi r^2} d\gamma dr \\
&= 2\pi\lambda \int_0^{\infty} \sum_{m=1}^{M} \alpha_m \left[\int_0^{\infty} Q\left(\sqrt{\frac{2\beta_m \gamma}{\tilde{\mu}_0 r^{\tilde{\mu}_1} e^{\tilde{\mu}_2 r}}} \right) \right. \\
&\quad \left. \times e^{-\gamma} d\gamma \right] r e^{-\lambda\pi r^2} dr. \qquad (28)
\end{aligned}$$

The inner integral in (28) can be solved by parts in closed-form, yielding

$$\begin{aligned}
P_{\mathcal{E}} &= 2\pi\lambda \int_0^{\infty} \sum_{m=1}^{M} \alpha_m \\
&\quad \times \frac{1}{2} \left(1 - \sqrt{\frac{\beta_m}{\tilde{\mu}_0 r^{\tilde{\mu}_1} e^{\tilde{\mu}_2 r} + \beta_m}} \right) r e^{-\lambda\pi r^2} dr, \qquad (29)
\end{aligned}$$

which after some manipulation can be written as in (27). □

IV. NUMERICAL RESULTS

In this section numerical results are presented to investigate the effect of rainfall and SDS on the performance of cellular downlink. Throughout this section, we assume a noise PSD of $N_0 = -70$ dBm ($N_0 = 10^{-7}$ mw) a bandwidth of $BW = 2600$ MHz (Band 7 - Telstra / Optus for 4G), and, for coverage calculations, a threshold $T = 0.01$, unless otherwise stated.

TABLE 2. Parameters of rain effect for different frequencies [40].

Frequency	a_{Rain}	b_{Rain}
24 GHz	0.1425	1.0101
28 GHz	0.2051	0.9679
38 GHz	0.4001	0.8816
75 GHz	1.1048	0.7221

The parameters in (11) are borrowed from Table 1 for $h_{\mathrm{BS}} = 7$ m and $h_{\mathrm{UE}} = 1.5$ m, where $h_{\mathrm{BS}}, h_{\mathrm{UE}}$ represent the heights of BS and UE, respectively. Also, parameters of rain effect for horizontal polarization at 24, 28, 38 and 75 GHz are listed in Table 2 [40], while for SDS, ϵ^*_{sd} values for different frequencies are taken from Table 3 [32] and find ϵ^*_{eq} for different visibility values, V, via (3) and (4) for $m_d = 9.43 \times 10^{-9}$ and $\rho_s = 1.07$ [32], which are used to obtain the SDS related path-loss $\zeta_{k,dB}(r)$ in (5).

Fig. 2 shows the average coverage probability degradation due to SDS/rainfall, defined as the difference between coverage probability with and without SDS/rainfall conditions. The summations in (16) are truncated to 15 terms, as higher k and j values in the summations indexes have a negligible effect on results. It can be observed that, as expected, either decreasing SDS visibility, in Fig. 2a, or increasing rain rate, in Fig. 2b, increase attenuation and hence decrease coverage. On the other hand, increasing λ decreases the distance of users to their corresponding BS. Since the attenuation due to SDS and rainfall, as well as the path loss, are related to distance, increasing λ reduces the loss. For instance, comparing the curves in Fig. 2a corresponding to $\lambda = 0.001$ and $\lambda = 0.005$ for a SDS visibility of 10^{-1} km, reveals that the coverage probability is 0.62 less than the case of clear weather (no SDS) for $\lambda = 0.001$, i.e., $\Delta P_{\mathcal{C}} = 0.62$. However, when a larger number of BSs are deployed (i.e., $\lambda = 0.005$), users will be served by BSs which are closer to them; therefore, the loss of coverage probability reduces to 0.26. In the case of rainfall, for $\lambda = 0.001$ it can be observed in Fig. 2b that

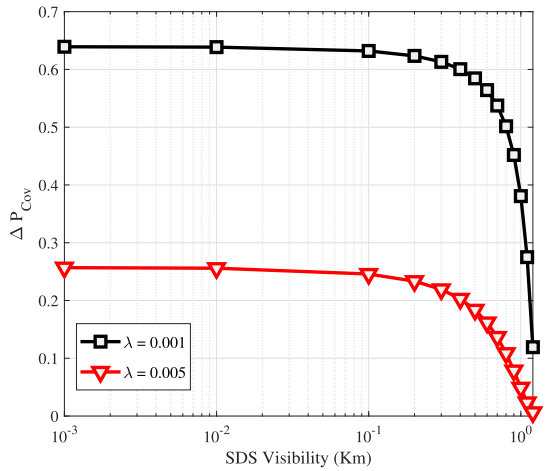

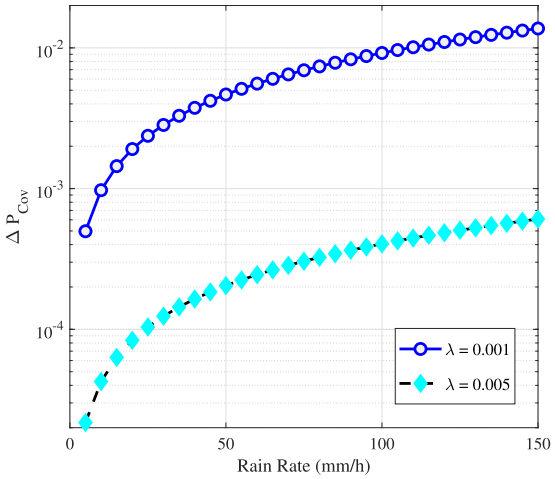

(a) ΔP_{cov} vs. SDS visibility, with $T = 0.01$, $P = 20$ W and $N_0 = 10^{-10}$ W.

(b) ΔP_{cov} vs. rainfall rate, with $T = 0.01$, $P = 20$ W and $N_0 = 10^{-10}$ W.

FIGURE 2. Coverage degradation probability due to SDS/rainfall.

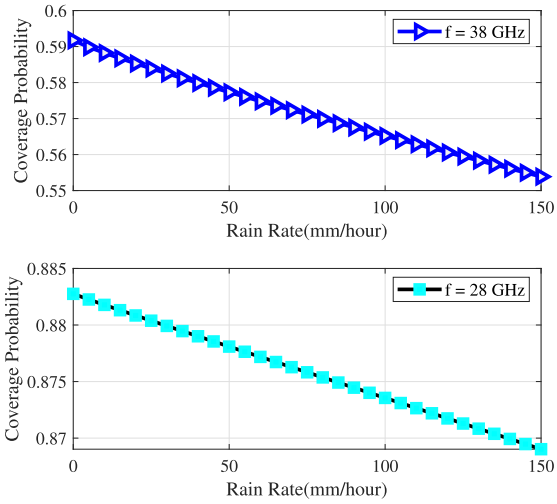

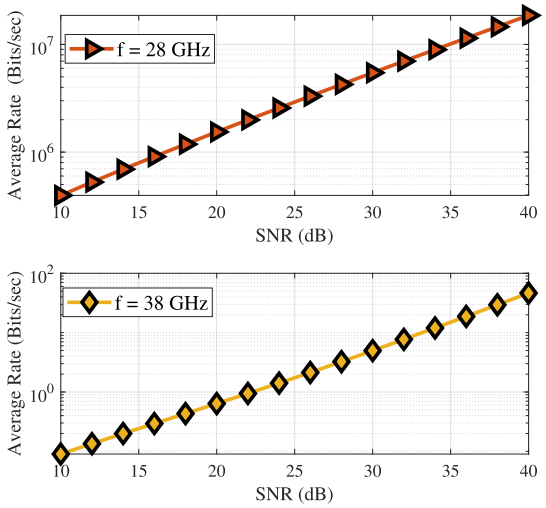

(a) Coverage probability for different rainfall rates, with $\lambda = 0.001$, $T = 0.01$, $P = 20$ W and $N_0 = 10^{-10}$ W.

(b) Average rate vs. SNR for SDS conditions for different frequencies with $\lambda = 0.05$ and $V = 0.05$ Km.

FIGURE 3. Coverage probability and average rate versus rainfall rate (in rain conditions) and SNR (in SDS conditions) for 28 and 38 GHz.

TABLE 3. Complex permittivities of SDS for different frequencies [32].

Frequency	$\epsilon^*_{sd} = \epsilon'_{sd} - j\epsilon''_{sd}$
24 GHz	3.6-j0.65
37 GHz	4.0-j1.3
100 GHz	3.5-j1.64

$\Delta P_{\mathcal{C}} = 0.009$, while for $\lambda = 0.005$, $\Delta P_{\mathcal{C}} = 0.0004$, which represents more than an order of magnitude difference with respect to the former case.

Fig. 3 shows coverage and average rate as a function of rainfall rate and average SNR, respectively, considering 28 and 38 GHz. Fig. 3a depicts the coverage probability versus rainfall rate. It is observed that, for both frequencies, the coverage probability decreases with increasing rainfall rate, showing a higher slope for 38 GHz. For instance, for a rainfall rate of $\tilde{R} = 50$ mm/h, the coverage probabilities at $f = 28$ GHz and $f = 38$ GHz are $P_{\mathcal{C}} = 0.878$ and $P_{\mathcal{C}} = 0.578$, respectively. Also, comparing the results at $\tilde{R} = 150$ mm/h and $\tilde{R} = 0$ mm/h (no rainfall) reveals that for the case of $f = 28$ GHz, the coverage probability decreases 0.015 (from 0.884 in $\tilde{R} = 0$ to 0.869 in $\tilde{R} = 150$). However, this degradation is higher (around 0.035) at $f = 38$ GHz. Fig. 3b shows the average achievable bit rate vs. SNR considering SDS. It can be seen that the average achievable bit rate is considerably reduced by as much as 6 orders of magnitude when the frequency increases from 28 to 38 GHz. To obtain the average throughput results of this figure, $\lambda = 0.05$, $V = 0.05$ km for SDS and Bandwidth = 2600 MHz (Band 7 - Telstra / Optus for 4G) have been considered.

Fig. 4 shows the excess transmission power, referred to as cost, required to reach a target coverage probability in the

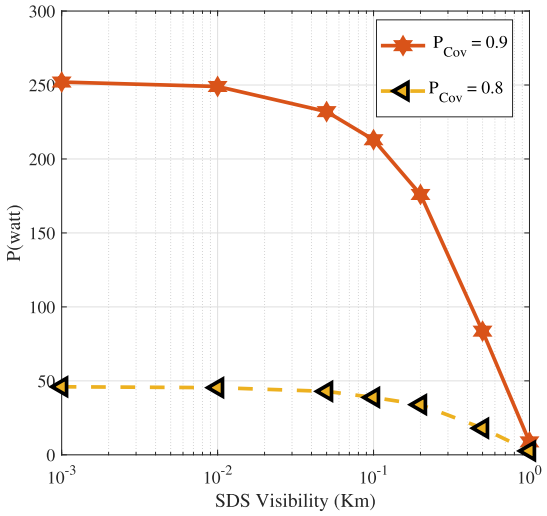

(a)Costs of system vs. SDS visibility, with $\lambda = 0.005$, $N_0 = 10^{-10}$ W, and $T = 0.01$.

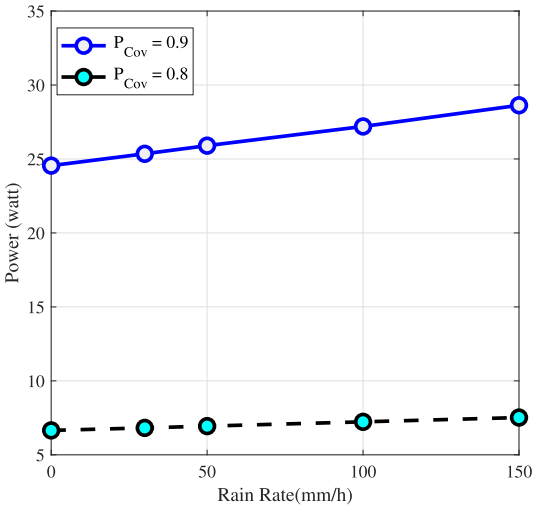

(b)Costs of system vs. rainfall rate, with $\lambda = 0.005$, $N_0 = 10^{-10}$ W, and $T = 0.01$.

FIGURE 4. Power costs due to SDS/rainfall attenuation.

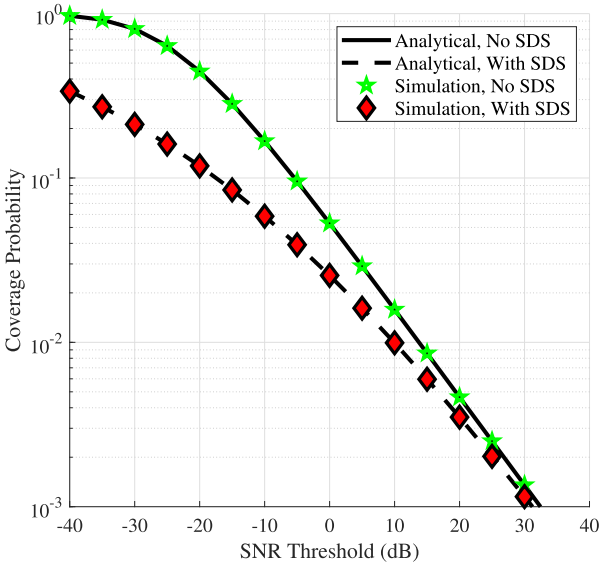

FIGURE 5. Average coverage probability vs. target SNR threshold, with $\lambda = 0.001$, $P = 1$ W, $N_0 = 10^{-10}$ W and $V = 0.05$ Km for SDS in $f = 28$ GHz.

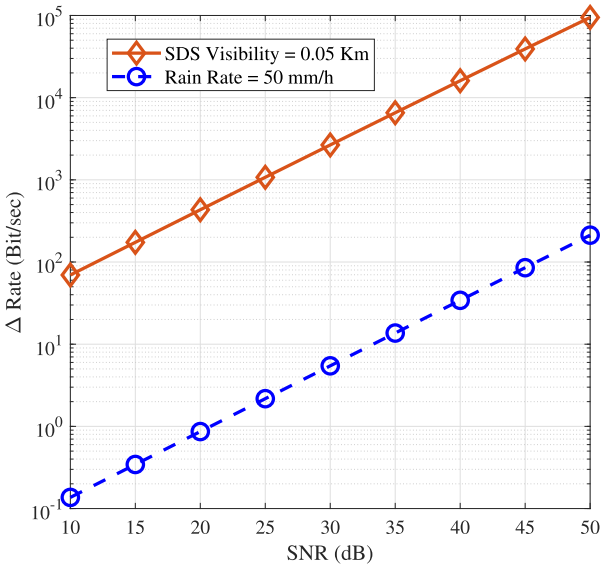

FIGURE 6. Degradation of average maximum achievable bit rate vs. SNR (dB) for $f = 28$ GHz, $\lambda = 0.001$ and bandwidth of 2600 MHz (Band 7 - Telstra / Optus for 4G).

presence of SDS and rain, with respect to the power required in clear sky conditions. Fig. 4a shows the cost with respect to visibility for an SDS scenario. As an example, for target coverage probabilities of 0.8 and 0.9, considering 10^{-2} km visibility, the power costs are 50 and 250 watts, respectively. On the other hand, Fig. 4b shows that, at a rainfall rate of 50 mm/h, increasing the target coverage probability from 0.8 to 0.9 leads to an almost 5-fold increase in power cost. Comparison between Figs. 4a and 4b also suggests that the SDS effect is more significant than the rain effect and will impose a higher cost to the system.

Fig. 5 compares analytical and simulation results of coverage probability *vs.* SNR threshold for SDS and clear sky conditions. As it be can seen in the figure, analytical results agrees with simulations. It can also be observed that the coverage degradation due to SDS is more significant at low SNR thresholds. Fig. 6 depicts the average rate degradation due to SDS and rainfall for 0.05 km visibility and 50 mm/h rainfall rate, respectively. Results show that, for severe weather conditions, the average rate degradation due to SDS is considerably higher than that due to rain.

The average bit error rate in the presence of SDS/rainfall is represented in Fig. 7 for BPSK modulation computed from

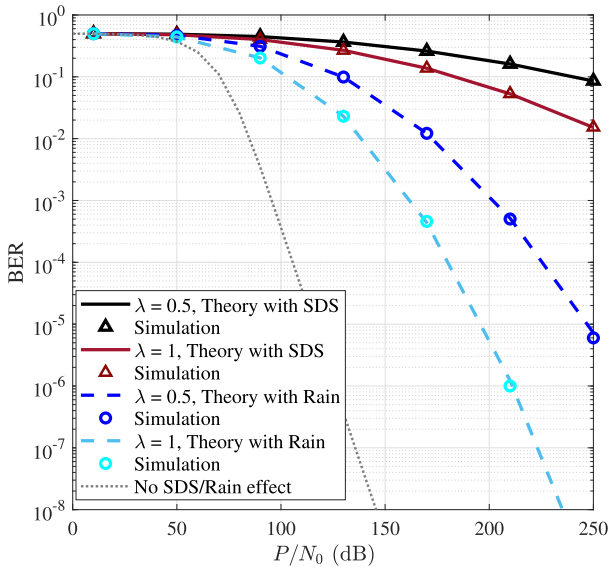

FIGURE 7. Average BER in the presence of SDS/Rain at $f = 28$ GHz with BPSK modulation, path loss parameters $B = 3.73$, $A = 75.85$ dB, $V = 1$ km, $\tilde{R} = 50$ mm/h, and $\lambda = 0.5$ for the case no SDS/Rain.

(27) with $M = 1$, $\alpha_1 = 1$ and $\beta_1 = 2$. The exact average BER versus the signal power to noise ratio (P/N_0) is plotted for different values of cell density ($\lambda = 0.5, 1$) and verified by Monte-Carlo simulations. It can be observed that increasing the cell density yields lower BER, due to the reduced average distance of users to their serving BS. The figure also shows that the obtained BER in SDS condition is higher than under rainfall, and both of them are significantly worse (higher BER) than the "No SDS/Rain" case, when the signal is only weakened by path loss.

V. CONCLUSION

In this paper, the effect of sand and dust storms (SDSs) and rainfalls on the performance of cellular networks in the mm-Wave band is investigated. A novel unified mathematical framework has been presented in order to analyze the power cost that the system has to pay to overcome the counterproductive effects of these atmospheric phenomena so that the same performance is achieved as in clear weather. Specifically, we focused on coverage probability, average achievable rate and average BER of the system and provided exact expressions for the performance degradation. Numerical results were provided to study the effects of various parameters, including the density of deployed cells, visibility (in SDS conditions) and rainfall rate (in rain conditions). The presented results show that, when comparing severe rain (high rain rate) with severe SDS (low visibility), the loss of performance in SDS is higher than in the case of rainfall. This is in agreement with the results presented in [31], where SDS attenuation is compared with rain and gaseous attenuation at 22 GHz, and it is shown that SDS attenuation is much higher than others. It must be remarked that rainfall and SDS attenuation modeling for 5G/6G frequency bands, including mm-Wave and Teraherz, is an open research area, and the proposed mathematical framework is expected to provide a useful tool where different attenuation models can be tested at the network level. Such comparison is left for future research.

APPENDIX
PROOF OF PROPOSITION 1

Proof: To obtain the coverage probability we can write

$$P_{\mathcal{C}}(T) = \mathbb{E}\{\Gamma_k > T|r\} \tag{30a}$$

$$= \int_{r>0} \Pr\left\{\frac{P|h_{w,k}|^2}{N_0 10^{L_{k,\mathrm{dB}}(r)/10}} > T|r\right\} f_R(r)dr \tag{30b}$$

$$= \int_0^\infty \Pr\left\{|h_{k,w}|^2 > \frac{TN_0}{P} 10^{L_{k,\mathrm{dB}}(r)/10}|r\right\} f_R(r)dr \tag{30c}$$

$$= \int_0^\infty 2\pi\lambda r \exp\left(-\frac{TN_0}{P} 10^{L_{k,\mathrm{dB}}(r)/10}\right) \times \exp\left(-\lambda\pi r^2\right) dr. \tag{30d}$$

Note that substituting $L_{k,\mathrm{dB}}(r)$ from (12) yields

$$10^{L_{k,\mathrm{dB}}(r)/10} = 10^{\mathcal{L}_c/10 + \mathcal{L}_l r/10 + \mathcal{L}_{lg}\ln(r)/10} = 10^{\mathcal{L}_c/10} \exp\left[\ln(10)\mathcal{L}_l r/10\right] \times r^{\ln(10)\mathcal{L}_{lg}/10}. \tag{31}$$

In (30), we assume that $|h_{k,w}|$ and $|h_{k,w}|^2$ follow Rayleigh and exponential distributions, respectively. By substituting (31) into (30d) we have

$$P_{\mathcal{C}}(T) = \int_0^\infty \exp\left[-\mu_0 r^{\mu_1} \exp(\mu_2 r) - \pi\lambda r^2\right] 2\pi\lambda r dr. \tag{32}$$

We then use the exponential series, $e^x = \sum_{k=0}^{\infty} \frac{x^k}{k!}$ to solve the integral in (32), where

$$\exp\left(-\mu_0 r^{\mu_1} \exp(\mu_2 r)\right) = \sum_{k=0}^{\infty}\sum_{j=0}^{\infty} \frac{(-\mu_0)^k (k\mu_2)^j}{k!j!} r^{k\mu_1 + j}, \tag{33}$$

then the integral in (32) can be rewritten as

$$P_{\mathcal{C}}(T) = \sum_{k=0}^{\infty}\sum_{j=0}^{\infty} \frac{(-\mu_0)^k (k\mu_2)^j}{k!j!} \int_0^\infty r^{k\mu_1 + j} \times 2\pi r\lambda \times \exp(-\lambda\pi r^2) dr \tag{34}$$

$$= \sum_{k=0}^{\infty}\sum_{j=0}^{\infty} \frac{(-\mu_0)^k (k\mu_2)^j}{k!j!} (\lambda\pi)^{-\frac{k\mu_1 + j}{2}} \Gamma\left(\frac{k\mu_1 + j + 2}{2}\right). \tag{35}$$

The coverage probability without SDS and rain effects (clear sky conditions) is then obtained by setting $\mu_2 = 0$ as

$$\hat{P}_{\mathcal{C}}(T) = \sum_{k=0}^{\infty} \frac{(-\mu_0)^k}{k!} (\lambda\pi)^{-\frac{k\mu_1}{2}} \Gamma\left(\frac{k\mu_1 + 2}{2}\right). \tag{36}$$

And subtracting (35) from (36) completes the proof. □

REFERENCES

[1] S. A. Busari, S. Mumtaz, S. Al-Rubaye, and J. Rodriguez, "5G millimeter-wave mobile broadband: Performance and challenges," *IEEE Commun. Mag.*, vol. 56, no. 6, pp. 137–143, Jun. 2018.

[2] N. Xia, H. Chen, and C. Yang, "Radio resource management in machine-to-machine communications—A survey," *IEEE Commun. Surveys Tuts.*, vol. 20, no. 1, pp. 791–828, 1st Quart., 2018.

[3] R. I. Ansari, C. Chrysostomou, S. A. Hassan, M. Guizani, S. Mumtaz, J. Rodriguez, and J. J. P. C. Rodrigues, "5G D2D networks: Techniques, challenges, and future prospects," *IEEE Syst. J.*, vol. 12, no. 4, pp. 3970–3984, Dec. 2018.

[4] R. Olsen, D. Rogers, and D. Hodge, "The aR^b relation in the calculation of rain attenuation," *IEEE Trans. Antennas Propag.*, vol. AP-26, no. 2, pp. 318–329, Mar. 1978.

[5] D. Nandi and A. Maitra, "Study of rain attenuation effects for 5G mm-wave cellular communication in tropical location," *IET Microw., Antennas Propag.*, vol. 12, no. 9, pp. 1504–1507, Jul. 2018.

[6] H. Desa, M. Sofian, and Z. Shaiful, "Study of integration 2.4 GHz and 5.8 GHz in RFID tag," in *Proc. Int. Conf. Man-Mach. Syst. (ICoMMS)*, Oct. 2009, pp. 1–12.

[7] Y. Zhang, P. Wang, and A. Goldsmith, "Rainfall effect on the performance of millimeter-wave MIMO systems," *IEEE Trans. Wireless Commun.*, vol. 14, no. 9, pp. 4857–4866, Sep. 2015.

[8] *Characteristics of Precipitation for Propagation Modelling*, document 837-6, ITU-R, 2012.

[9] K. S. Paulson, "Estimating 1 min rain rate distributions from numerical weather prediction," *Radio Sci.*, vol. 52, no. 1, pp. 176–184, Jan. 2017, doi: 10.1002/2016RS006111.

[10] K. S. Paulson, C. Ranatunga, and T. Bellerby, "A method to estimate trends in distributions of 1 min rain rates from numerical weather prediction data," *Radio Sci.*, vol. 50, no. 9, pp. 931–940, Sep. 2015, doi: 10.1002/2015RS005651.

[11] L. D. S. Mello, M. S. Pontes, I. Fagundes, M. P. C. Almeida, and F. J. A. Andrade, "Modified rain attenuation prediction method considering the effect of wind direction," *J. Microw., Optoelectron. Electromagn. Appl.*, vol. 13, no. 2, pp. 254–267, Dec. 2014.

[12] F. Norouzian, E. Marchetti, M. Gashinova, E. Hoare, C. Constantinou, P. Gardner, and M. Cherniakov, "Rain attenuation at millimeter wave and low-THz frequencies," *IEEE Trans. Antennas Propag.*, vol. 68, no. 1, pp. 421–431, Jan. 2020.

[13] I. Shayea, T. A. Rahman, M. H. Azmi, and M. R. Islam, "Real measurement study for rain rate and rain attenuation conducted over 26 GHz microwave 5G link system in Malaysia," *IEEE Access*, vol. 6, pp. 19044–19064, 2018.

[14] I. Shayea, T. A. Rahman, M. H. Azmi, and A. Arsad, "Rain attenuation of millimetre wave above 10 GHz for terrestrial links in tropical regions," *Trans. Emerg. Telecommun. Technol.*, vol. 29, no. 8, p. e3450, Aug. 2018.

[15] I. Shayea, L. A. Nissirat, M. A. Nisirat, A. Alsamawi, T. A. Rahman, M. H. Azmi, M. Abo-Zeed, and I. Trrad, "Rain attenuation and worst month statistics verification and modeling for 5G radio link system at 26 GHz in Malaysia," *Trans. Emerg. Telecommun. Technol.*, vol. 30, no. 12, pp. 1–12, Dec. 2019.

[16] A. A. Budalal, I. Shayea, Md. R. Islam, M. H. Azmi, H. Mohamad, S. A. Saad, and Y. I. Daradkeh, "Millimetre-wave propagation channel based on NYUSIM channel model with consideration of rain fade in tropical climates," *IEEE Access*, vol. 10, pp. 1990–2005, 2022.

[17] A. A. Budalal and M. R. Islam, "Path loss models for outdoor environment—With a focus on rain attenuation impact on short-range millimeter-wave links," *E-Prime-Adv. Electr. Eng., Electron. Energy*, vol. 3, Mar. 2023, Art. no. 100106.

[18] J. Huang, Y. Cao, X. Raimundo, A. Cheema, and S. Salous, "Rain statistics investigation and rain attenuation modeling for millimeter wave short-range fixed links," *IEEE Access*, vol. 7, pp. 156110–156120, 2019.

[19] A. M. Al-Samman, M. Mohamed, Y. Ai, M. Cheffena, M. H. Azmi, and T. A. Rahman, "Rain attenuation measurements and analysis at 73 GHz E-band link in tropical region," *IEEE Commun. Lett.*, vol. 24, no. 7, pp. 1368–1372, Jul. 2020.

[20] *Beyond Scarcity: Water Security in the Middle East and North Africa*, MENA Development Report, World Bank, Washington, DC, USA, 2018. [Online]. Available: https://openknowledge.worldbank.org/handle/10986/27659

[21] P. Procházka, V. Hönig, M. Maitah, I. Pljuća, and J. Kleindienst, "Evaluation of water scarcity in selected countries of the Middle East," *Water*, vol. 10, no. 10, p. 1482, Oct. 2018.

[22] R. Papi, A. A. Kakroodi, M. Soleimani, L. Karami, F. Amiri, and S. K. Alavipanah, "Identifying sand and dust storm sources using spatial–temporal analysis of remote sensing data in central Iran," *Ecol. Informat.*, vol. 70, Sep. 2022, Art. no. 101724.

[23] S. Ghobrial and S. Sharief, "Microwave attenuation and cross polarization in dust storms," *IEEE Trans. Antennas Propag.*, vol. AP-35, no. 4, pp. 418–425, Apr. 1987.

[24] M. Chiou and J. Kiang, "Attenuation of millimeter-wave in a sand and dust storm," *IEEE Geosci. Remote Sens. Lett.*, vol. 13, no. 8, pp. 1094–1098, Aug. 2016.

[25] T. S. Chu, "B.S.T.J. Brief: Effects of sandstorms on microwave propagation," *Bell Syst. Tech. J.*, vol. 58, no. 2, pp. 549–555, Feb. 1979.

[26] A. S. Ahmed, A. A. Ali, and M. A. Alhaider, "Airborne dust size analysis for tropospheric propagation of millimetric waves into dust storms," *IEEE Trans. Geosci. Remote Sens.*, vol. GE-25, no. 5, pp. 593–599, Sep. 1987.

[27] Z. Elabdin, M. R. Islam, O. O. Khalifa, H. Essam A. Raouf, and M. J. E. Salami, "Development of mathematical model for the prediction of microwave signal attenuation due to duststorm," in *Proc. Int. Conf. Comput. Commun. Eng.*, May 2008, pp. 1156–1161.

[28] S. M. Sharif, "Attenuation properties of dusty media using MIE scattering solution," *Prog. Electromagn. Res. M*, vol. 43, pp. 9–18, 2015.

[29] M. R. Islam, Z. E. O. Elshaikh, O. O. Khalifa, A. Z. Alam, S. Khan, and A. W. Naji, "Prediction of signal attenuation due to duststorms using MIE scattering," *IIUM Eng. J.*, vol. 11, no. 1, pp. 71–87, May 2010.

[30] E. A. A. Elsheikh, Md. R. Islam, M. H. Habaebi, A. F. Ismail, and A. Zyoud, "Dust storm attenuation modeling based on measurements in Sudan," *IEEE Trans. Antennas Propag.*, vol. 65, no. 8, pp. 4200–4208, Aug. 2017.

[31] H. S. Cankurtaran, S. Yarkan, M. O. Hasna, and K. A. Qaraqe, "Statistical modeling of sand and dust storm attenuation," in *Proc. Int. Balkan Conf. Commun. Netw. (BalkanCom)*, Aug. 2022, pp. 95–99.

[32] X. Dong, H. Chen, and D. Guo, "Microwave and millimeter-wave attenuation in sand and dust storms," *IEEE Antennas Wireless Propag. Lett.*, vol. 10, pp. 469–471, 2011.

[33] H. Zhang, S. Chen, L. Feng, Y. Xie, and L. Hanzo, "A universal approach to coverage probability and throughput analysis for cellular networks," *IEEE Trans. Veh. Technol.*, vol. 64, no. 9, pp. 4245–4256, Sep. 2015.

[34] H. Wang, X. Zhou, and M. C. Reed, "Coverage and throughput analysis with a non-uniform small cell deployment," *IEEE Trans. Wireless Commun.*, vol. 13, no. 4, pp. 2047–2059, Apr. 2014.

[35] E. M. Abuhdima and I. M. Saleh, "Effect of sand and dust storms on GSM coverage signal in southern Libya," in *Proc. Int. Conf. Electron. Devices, Syst. Appl.*, Apr. 2010, pp. 264–268.

[36] G. N. Kamga and S. Aïssa, "Wireless power transfer in mmWave massive MIMO systems with/without rain attenuation," *IEEE Trans. Commun.*, vol. 67, no. 1, pp. 176–189, Jan. 2019.

[37] A. Hilario-Tacuri and A. Tamo, "BER performance of mm-wave based systems in rainfall scenarios," in *Proc. IEEE 25th Int. Conf. Electron., Electr. Eng. Comput. (INTERCON)*, Aug. 2018, pp. 1–4.

[38] H. ElSawy, E. Hossain, and M. Haenggi, "Stochastic geometry for modeling, analysis, and design of multi-tier and cognitive cellular wireless networks: A survey," *IEEE Commun. Surveys Tuts.*, vol. 15, no. 3, pp. 996–1019, 3rd Quart., 2013.

[39] M. Haenggi, "On distances in uniformly random networks," *IEEE Trans. Inf. Theory*, vol. 51, no. 10, pp. 3584–3586, Oct. 2005.

[40] *Specific Attenuation Model for Rain for Use in Prediction Methods*, document 838-3, ITU-R, 2005.

[41] M. C. Kestwal, S. Joshi, and L. S. Garia, "Prediction of rain attenuation and impact of rain in wave propagation at microwave frequency for tropical region (Uttarakhand, India)," *Int. J. Microw. Sci. Technol.*, vol. 2014, pp. 1–6, Jun. 2014.

[42] *Characteristics of Precipitation for Propagation Modeling. Recommendation ITU-R*, ITU, Geneva, Switzerland, 2017.

[43] G. J. Proakis, M. Salehi, N. Zhou, and X. Li, *Communication Systems Engineering*, vol. 2. Upper Saddle River, NJ, USA: Prentice-Hall, 1994.

[44] G. R. MacCartney, J. Zhang, S. Nie, and T. S. Rappaport, "Path loss models for 5G millimeter wave propagation channels in urban microcells," in *Proc. IEEE Global Commun. Conf. (GLOBECOM)*, Atlanta, GA, USA, Dec. 2013, pp. 3948–3953.

[45] A. Goldsmith, *Wireless Communications*. Cambridge, U.K.: Cambridge Univ. Press, 2005.
[46] M. Abramowitz and I. A. Stegun, *Handbook of Mathematical Functions: With Formulas, Graphs, and Mathematical Tables*. North Chelmsford, MA, USA: Courier Corporation, 1965.
[47] F. Javier López-Martínez, E. Martos-Naya, J. F. Paris, and U. Fernández-Plazaola, "Generalized BER analysis of QAM and its application to MRC under imperfect CSI and interference in Ricean fading channels," *IEEE Trans. Veh. Technol.*, vol. 59, no. 5, pp. 2598–2604, Jun. 2010.

MARYAM OLYAEE received the B.Sc. degree in electrical engineering from Shahed University, Tehran, Iran, in 2014, and the M.Sc. and Ph.D. degrees in electrical engineering from the Shiraz University of Technology, Shiraz, Iran, in 2016 and 2021, respectively. She was a Postdoctoral Researcher with the University of Malaga, Spain, from March 2021 to August 2022, and the University of Granada, Spain, from September 2022 to February 2023. She is currently a Senior Researcher with the University of Malaga. Her research interests include wireless and cellular communications, multiuser MIMO/MIMO-OFDM, massive MIMO systems, reconfigurable intelligent surfaces (RIS), green communications, and mm-Wave communications for 5G and beyond.

MOHSEN ESLAMI received the B.Sc. and M.Sc. degrees in electrical engineering from the University of Tehran, Tehran, Iran, in 2000 and 2002, respectively, and the Ph.D. degree in electrical engineering from the University of Alberta, Edmonton, AB, Canada, in 2009. He was a Postdoctoral Fellow with the Department of Electrical and Computer Engineering, University of Alberta, from 2009 to 2011. He is currently an Associate Professor with the Department of Electrical and Electronics Engineering, Shiraz University of Technology. His research interests include wireless communications, multiple antenna systems, cooperative communications, and mm-Wave communications.

KEIVAN NAVAIE (Senior Member, IEEE) is a Principal and AI Technology Advisor at the Information Commissioner Office (U.K. Data Protection Regulatory Body), and a Chair Professor in Intelligent Networks at the School of Computing and Communications, Lancaster University. He has an interdisciplinary research portfolio seeking innovative solutions to address fundamental technical and design challenges in intelligent cyber-physical systems and their applications in reducing carbon-foot print in day-to-day life activities. His research topics include deep learning, privacy enhanced AI, AI regulations, distributed and federated AI, connectivity resilience incyber-physical systems and the IoT, machine learning and artificial intelligence applications, cognitive communications networks, and cryptosystems. He has actively contributed to evidence-based policymaking through involvement with the United Nations' International Telecommunications Union (ITU), EU Environment Agency, Information Commissioner's Office, and EU Parliament. He is a Fellow of IET, a Chartered Engineer in the U.K., and a Senior Fellow of the HEA. He is on the editorial board of the IEEE TRANSACTIONS ON WIRELESS COMMUNICATIONS, the IEEE COMMUNICATIONS SURVEYS AND TUTORIAL, and the IEEE Communication Letters.

JUAN M. ROMERO-JEREZ (Senior Member, IEEE) received the M.Sc. degrees in telecommunications engineering and mathematics and the Ph.D. degree in telecommunications engineering from the University of Malaga, Spain, in 2001. In 1996, he joined the Department of Electronic Technology, University of Malaga, where he is currently a Full Professor. He was a Visiting Associate Professor with the Department of Electrical Engineering, Stanford University, from September 2005 to February 2006, from September 2007 to February 2008, and from February 2016 to March 2016. He has participated in several research projects in the areas of packet radio transmission, multiple antennas, interference management, and cellular networks. His current research interests include wireless communications and, more specifically: wireless communications performance analysis, multipath fading, wireless channel modeling, diversity systems, smart antennas, MIMO performance, and interference management. He was an Editor of the IEEE TRANSACTIONS ON WIRELESS COMMUNICATIONS from 2015 to 2020 and the General Co-Chair of the 2022 IEEE Communication Theory Workshop (CTW 2022).

HADI HASHEMI received the B.Sc. degree in electrical engineering from Urmia University, in 2012, the M.Sc. degree in electrical engineering from Imam Khomeini International University, in 2014, and the Ph.D. degree in communications from the Shiraz University of Technology, in 2021. He was a Visiting Researcher with the University of Malaga, Spain, from September 2022 to February 2023. He is currently a Postdoctoral Researcher with the University of Granada, Spain. His research interests include cooperative communications, wireless sensor networks, cognitive radio networks, channel modeling, satellite communication, and next generation mobile networks.

JAVAD HAGHIGHAT received the B.Sc. and M.Sc. degrees in electrical engineering from the University of Tehran, in 2000 and 2002, respectively, and the Ph.D. degree in electrical engineering from Concordia University, Montreal, Canada, in 2007. He is currently with the Department of Electrical and Electronics Engineering, TED University, Ankara, Turkey, as an Associate Professor. His research interests include source coding, channel coding, cooperative communications, and wireless sensor networks.

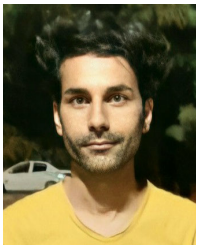

MOHAMAD BAHMANPOUR received the B.Sc. degree in electrical engineering-communications systems from the Shiraz University of Technology, Shiraz, Iran, in 2019. His research interests include the performance evaluation of telecommunication systems, millimeter wave communications, hyperspectral remote sensing imaging, deep neural networks, and pattern recognition.